Bull Volcanol (2015) 77: 87
DOI 10.1007/s00445-015-0972-5

RESEARCH ARTICLE

Groundmass crystallisation and cooling rates of lava-like ignimbrites: the Grey's Landing ignimbrite, southern Idaho, USA

B. S. Ellis[1] · **B. Cordonnier**[2] · **M. C. Rowe**[3] · **D. Szymanowski**[1] · **O. Bachmann**[1] · **G. D. M. Andrews**[4]

Received: 25 March 2015 / Accepted: 6 September 2015 / Published online: 16 September 2015
© Springer-Verlag Berlin Heidelberg 2015

Abstract Constraining magmatic and eruptive processes is key to understanding how volcanoes operate. However, reconstructing eruptive and pre-eruptive processes requires the ability to see through any post-eruptive modification of the deposit. The well-preserved Grey's Landing ignimbrite from the central Snake River Plain provides an opportunity to systematically investigate the post-eruptive processes occurring through a single deposit sheet. Despite overall compositional homogeneity in both bulk and glass compositions, the Grey's Landing ignimbrite does preserve differences in the abundance of Li in plagioclase crystals which are strongly associated with the host lithology. Li abundances in plagioclase from the quickly cooled upper and basal vitrophyres are typically low (average 5 ppm, n=262) while plagioclase from the microcrystalline interior of the deposit has higher Li contents (average 33 ppm, n=773). Given that no other trace elemental parameter in plagioclase varies, we interpret the variability in Li to reflect a post-depositional process. Groundmass crystallisation of a rhyolite like Grey's Landing requires ~50 % crystallisation of sanidine and variable amounts of a silica-rich phase (quartz, tridymite, cristobalite) and plagioclase to satisfy mass balance. We suggest the low affinity of Li for sanidine causes migration of groundmass Li into plagioclase during crystallisation. Even within the microcrystalline interior of the deposit, the morphology of the groundmass varies. The more marginal, finer-grained regions are dominated by cristobalite as the SiO_2-rich phase while tridymite and quartz are additionally found in the more slowly cooled, coarser-grained portions of thick sections of the ignimbrite. Numerical models of cooling and crystallisation tested against field observations indicate that the groundmass crystallisation occurred relatively rapidly following emplacement (a maximum of a few years where the ignimbrite is thickest). These numerical models also illustrate that the time at which the potential for rheomorphism ceases (either the ignimbrite is a solid glass, or >50 % crystalline) is diachronous across the deposit.

Keywords Rhyolite · Microcrystalline · Cooling rate · Numerical models · Ignimbrite · Lithium

Editorial handling: S. Self

Electronic supplementary material The online version of this article (doi:10.1007/s00445-015-0972-5) contains supplementary material, which is available to authorized users.

✉ B. S. Ellis
ben.ellis@erdw.ethz.ch

[1] Institute of Geochemistry and Petrology, ETH Zurich, NW Clausiusstrasse 25, 8092 Zurich, Switzerland

[2] Berninastrasse 45, 8090 Zürich, Switzerland

[3] School of Environment, University of Auckland, Commerce A Building, Private Bag 92019, Auckland 1142, New Zealand

[4] Department of Geosciences, California State University Bakersfield, Bakersfield, CA 93311, USA

Introduction

All volcanic deposits result from cooled magma with the cooling rate a first-order control on the texture of the resultant deposit. Where the rate of cooling outpaces the rate of nucleation, amorphous volcanic glass may be formed from melts of compositions ranging from basaltic (e.g. Pick and Tauxe 1993) to rhyolitic (e.g. Ross and Smith 1955). However, volcanic materials are commonly not glassy; rather, they are dominated by crystalline materials both in the form of phenocrysts and in microscopic grains.

Groundmass crystallisation may occur at restricted point sources (typically forming spherulites) or it may be pervasive. Spherulitic crystallisation has received a significant amount of attention with studies considering the composition, growth rate and localised changes in conditions surrounding spherulites (Castro et al. 2008, 2009; Watkins et al. 2009; Gardner et al. 2012). Pervasive groundmass crystallisation, despite being volumetrically many orders of magnitude more prevalent in lavas and rheomorphic ignimbrites than spherulite formation, has received relatively little attention (Rowe et al. 2012). Often, this microcrystalline material is referred to as 'devitrified'; however, we prefer to use the term microcrystalline as this removes the suggestion that the bulk of crystallisation occurred following the material solidifying into a glass.

The lack of attention paid to groundmass crystallisation is hindering the ability to derive reasonable models for many volcanic processes, from those occurring within the conduit to those that happen upon deposition. Crystallisation occurs rapidly, with andesitic dome samples from Montserrat becoming microcrystalline in a matter of days following extrusion (Baxter et al. 1999) and cristobalite and tridymite being reported from the Mount St. Helens and Chaitén domes (Cashman et al. 2008; Horwell et al. 2010). This rapid groundmass crystallisation causes significant changes in the physical properties of the material but has rarely been considered when attempting to model surficial processes such as the advance of lava flows or rheomorphism in ignimbrites. The degree of crystallinity and the morphology of the groundmass may also have important implications in terms of the relative stability of lava domes (Husain et al. 2014).

In this work, we combine a variety of geochemical and structural tools to characterise a high-grade, lava-like, welded ignimbrite from the Snake River Plain, Idaho. These measurements are made on samples from well-characterised sections of the Grey's Landing ignimbrite to observe differences in groundmass crystallinity through a deposit and the potential for such crystallisation processes to affect the composition of the deposit. The timing of such processes is then constrained with numerical models of rhyolite cooling and crystallisation.

Geological setting

The central Snake River Plain

The central Snake River Plain (CSRP) comprises part of the compositionally bimodal Columbia River-Yellowstone large igneous province which has been active for the past 17 Ma (Brueseke et al. 2008). The cause of the rhyolitic volcanism in the CSRP is commonly attributed to the Yellowstone hotspot (Geist and Richards 1993; Wolff et al. 2008) which currently underlies the Yellowstone volcanic field, Wyoming. Rhyolitic ignimbrites and lavas in the CSRP represent silicic volcanism between ~14 and 6 Ma, which has a general younging progression to the north-east (Fig. 1 inset). The rhyolitic ignimbrites in the CSRP are well-exposed at the margins of the plain in steep-sided canyons and fault scarps but are obscured by the later effusion of basalts within the plain itself.

Rhyolitic ignimbrites in the CSRP are considerably different to 'typical' rhyolitic ignimbrites (e.g. Bishop Tuff, Hildreth and Wilson 2007) and comprise a part of what Branney et al. (2008) termed 'Snake River (SR)-type' volcanism. The rhyolitic magmas are 'hot and dry' with magmatic temperatures inferred on the basis of numerous thermometers to be >850 °C (Ellis et al. 2010). The resultant ignimbrites are exceptionally well sorted, commonly lacking in lithic and pumice clasts and exhibit a bimodality of welding being either intensely welded or (rarely) non-welded. The welded ignimbrites are commonly lava-like and strongly rheomorphic despite having metaluminous bulk compositions (Branney et al. 2008; Andrews and Branney 2011).

The Grey's landing ignimbrite

Located in the Rogerson Graben, south of the city of Twin Falls, ID, the Grey's Landing ignimbrite is one of the best studied Snake River-type ignimbrites; it is exposed over an area of more than 400 km^2 and has an estimated eruption volume of ~20 km^3 (Fig. 1; Andrews et al. 2008; Andrews and Branney 2011). The ignimbrite changes in thickness markedly in response to pre-existing topography, reaching 75 m in thickness where it ponded in the half-graben and thinning to ~3 m thick where it feathered out against palaeotopography formed by north–south trending normal faults on the graben margins (Andrews et al. 2008).

Beneath the Grey's Landing ignimbrite, a 2-m thick succession of parallel-bedded fallout deposits (Fig. 2d) overlies a palaeosol developed in the underlying Backwaters Member (Fig. 2b). Within the Rogerson Graben, where the overlying ignimbrite is thick, the fallout succession has been fused into a solid glass by the heat and load of the overlying ignimbrite. Above the fallout, a black, glassy basal vitrophyre typically 2–3 m thick and containing cm-scale fiammé marks the beginning of the ignimbrite before passing into the crystallised interior which typifies the cores of CSRP ignimbrites and lavas (Branney et al. 2008; Andrews and Branney 2011; Fig. 2a). The contact between the basal vitrophyre and the crystallised interior is sharp. The crystallised interior of the ignimbrite is dominated by centimetre to decimetre-scale flow banding which picks out complex folds generated during rheomorphism (Fig. 2c; Andrews and Branney 2011). Commonly, the unit is sheet-jointed and dimple-jointed and exhibits extremely attenuated vesicles on the foliation planes. The top of the Grey's Landing ignimbrite is characterised by a thin, perlitic upper vitrophyre which is locally brecciated,

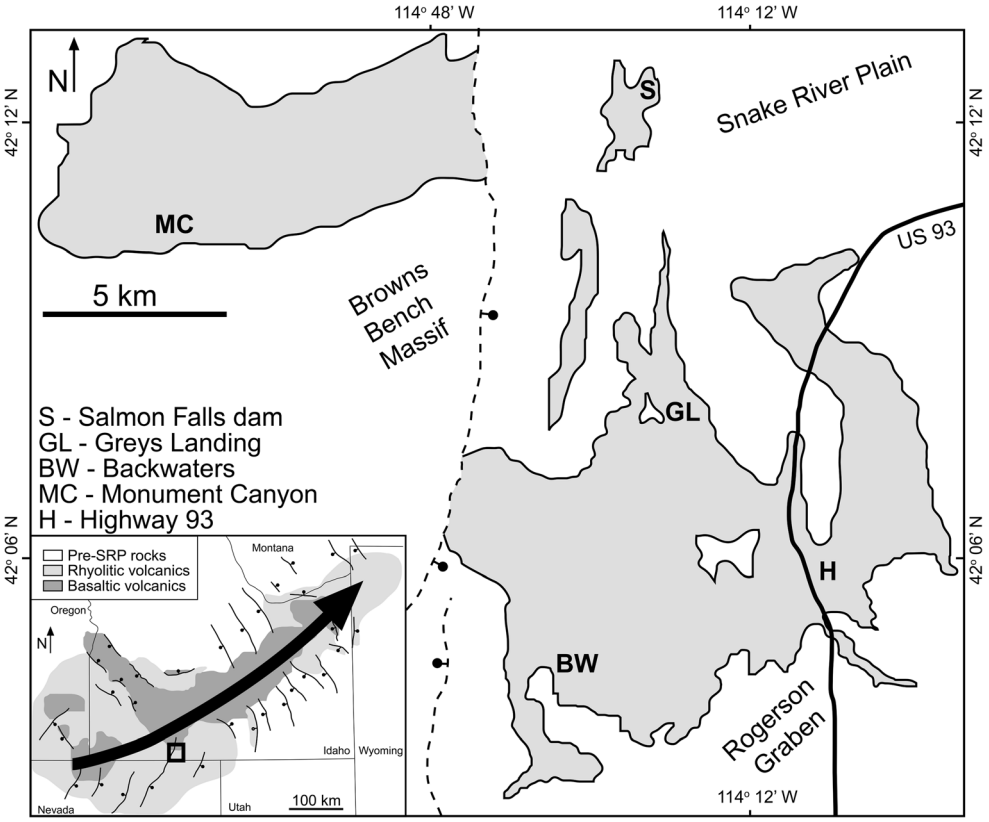

Fig. 1 Location map illustrating outcrop of the Grey's Landing ignimbrite after Andrews and Branney (2011). Abbreviations are: *BW* Backwaters, *GL* Grey's Landing, *S* Salmon Falls dam, *H* US highway 93, and *MC* Monument Canyon locations. *Inset* shows progression of volcanism along the Yellowstone–Snake River Plain province

and this is in turn overlain by a poorly to non-welded orange ash deposit which may represent a co-ignimbrite ashfall deposit. Where the ignimbrite is thin (<15 m), at the Monument Canyon location, at the contact between the upper vitrophyre and the crystallised interior numerous large (up to 10 cm), red spherulites occur.

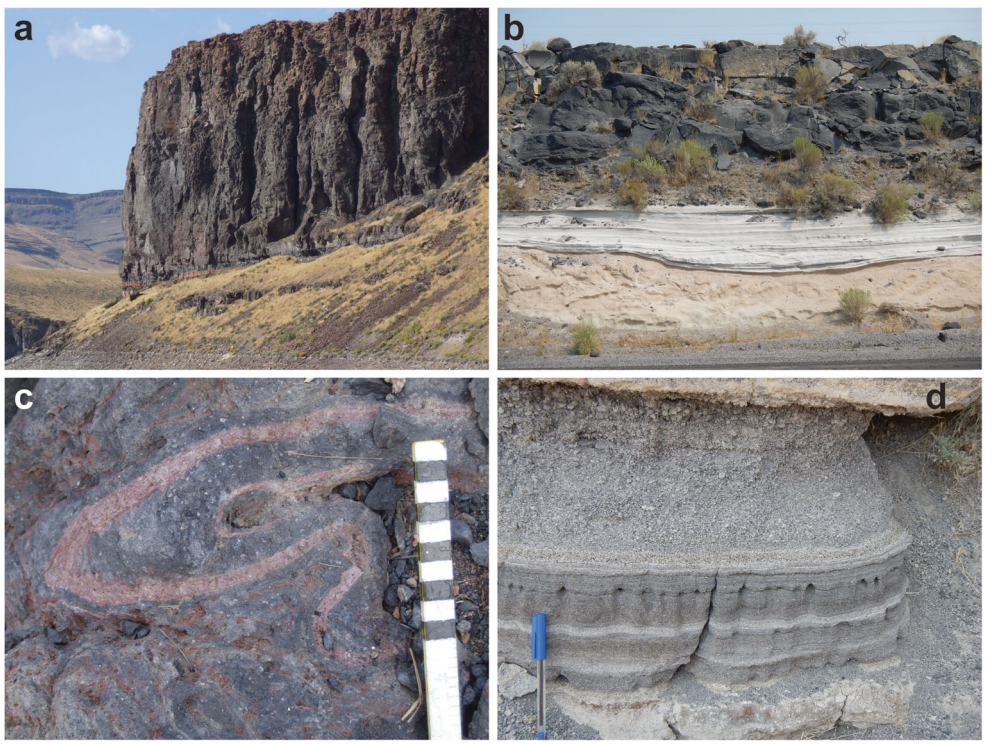

Fig. 2 Physical features of Grey's Landing ignimbrite. **a** Thick Grey's Landing ignimbrite at the BW location, with orange baked soil horizon visible near base of the cliff. **b** Thin, glassy Grey's Landing ignimbrite on eastern graben margin overlying volcaniclastic sediments and a palaeosol. **c** Rheomorphism in the upper vitrophyre of the ignimbrite. **d** Plinian fallout beneath the ignimbrite

Petrologically, the Grey's Landing ignimbrite is typical of the younger volcanic rocks from the CSRP with a phenocryst assemblage of rare quartz, plagioclase ($An_{35–45}$), augite, pigeonite, rare hypersthene, ilmenite, magnetite and accessory zircon and apatite (Andrews et al. 2008; Bonnichsen et al. 2008). Two-pyroxene thermometry suggests that the magmatic temperature of the Grey's Landing ignimbrite was approximately 950 °C (Andrews et al. 2008), comparable to other inferred magmatic temperatures for ignimbrites of the CSRP (Perkins and Nash 2002). As with all other rhyolites in the CSRP, the Grey's Landing exhibits a low-$\delta^{18}O$ signature indicative of assimilation of hydrothermally altered material during petrogenesis (Boroughs et al. 2012).

Methods

Samples were collected from vertical traverses at Grey's Landing, Backwaters, Salmon Falls dam, at Highway 93, and Monument Canyon sections (Fig. 1), originally described by Andrews and Branney (2011). The first three locations were used to provide a composite vertical section through the ignimbrite where it is thick (hereafter termed the Backwaters or BW section) while the Monument Canyon (hereafter MC) section and the Highway section (hereafter H) were used to characterise the ignimbrite where it thins against palaeotopography. Samples were analysed for bulk geochemistry via XRF and ICP in the Peter Hooper GeoAnalytical Laboratory at Washington State University using standard techniques. For major and trace elements, homogeneous powders were diluted 2:1 with di-lithium tetraborate flux, doubly fused and analysed on a ThermoARL XRF spectrometer. For trace and REE elements, the same powders were diluted 1:1 with di-lithium tetraborate flux before dissolution and analysis on an Agilent 7700 ICP-MS.

XRD analyses were carried out using Ni-filtered Cu$K\alpha$ (λ=1.54184 Å) radiation generated at 35 keV and 30 mA on a Siemens D500 X-ray diffractometer at Washington State University. XRD scans were run from 10–70° 2θ using a 0.05 step size and a 3-s dwell time. Using MDI Jade 8 software, diffraction patterns were processed with a 45-point Savitzky-Golay smoothing filter to reduce background (Wall et al. 2014). Both bulk (true whole rock) and picked groundmass separates were analysed. Relative crystallinity was calculated following the methodology described by Rowe et al. (2012) and Wall et al. (2014). A crystallinity calibration curve was generated to get an 'absolute' crystallinity using the same analytical conditions as the unknown samples (shown in Supplemental Material S1).

The relative proportions of silica polymorphs, cristobalite and tridymite, were quantified by comparing the count rate of the 100 % intensity peak (I100%) of each of the respective phases at a 2θ of 21.95° (cristobalite reference PDF# 077–8627) and 20.6° (tridymite reference PDF# 071–0261). Results of this method vary slightly dependent on the choice of XRD pattern—particularly in the case of tridymite where the I100% peak can change. In this scenario, calculated proportions should be viewed relatively. Potential overlap of diffraction patterns is also assessed by scaling a lower intensity peak free of interferences up to I100%. This procedure indicates that tridymite interference on the cristobalite I100% peak is minimal.

Groundmass characterisation and compositional mapping of polished rock billets was performed at ETH Zurich using a JEOL JSM-6390 scanning electron microscope equipped with Thermo UltraDry EDS detector at 15 kV. The spectral images recorded by the EDS system were analysed and used to create groundmass phase maps using the iSpectra toolbox (Liebske 2015).

Trace elements in plagioclase and glass were determined using LA-ICPMS with a 193 nm ArF Excimer laser from Resonetics coupled to a Thermo Element XR ICPMS within the Institute for Geochemistry and Petrology, ETH Zurich. Analytical conditions were identical to those described by Szymanowski et al. (2015) with spot sizes of 67 and 43 μm. Analyses are considered to have uncertainties of 5 % relative based upon long-term reproducibility of standards, and a full dataset including standards is provided in Supplemental Material.

Results

Mineralogy and textures

Crystallinity

Both groundmass and whole rock (bulk) crystallinity are calculated from X-ray powder diffraction results (Fig. 3). Bulk crystallinities are primarily used to constrain phenocryst abundances in glassy samples while groundmass results instead focus on microcrystalline products. All crystallinity results are provided in Supplemental Material. Orange ash above the upper vitrophyre is crystal-poor (~8.5 % bulk crystallinity and 2 % phenocrysts) consistent with an origin via fallout and crystal winnowing as suggested by Andrews and Branney (2011). Groundmass crystallinity of the 'thick' Backwaters section exhibits a stark difference between the vitrophyre (always <20 % crystalline) and microcrystalline samples (typically >80 %). Transitions between these zones are abrupt in the BW section where the transition from completely crystalline to glassy vitrophyre occurs over an interval of ~1 m. Calculated phenocryst contents (bulk groundmass crystallinity) indicate that the phenocryst content varies systematically through the section, with the lowest proportions (~2–5 %) in the interior of the section from 15 to 35 m height and the highest at the base (~9–12 %).

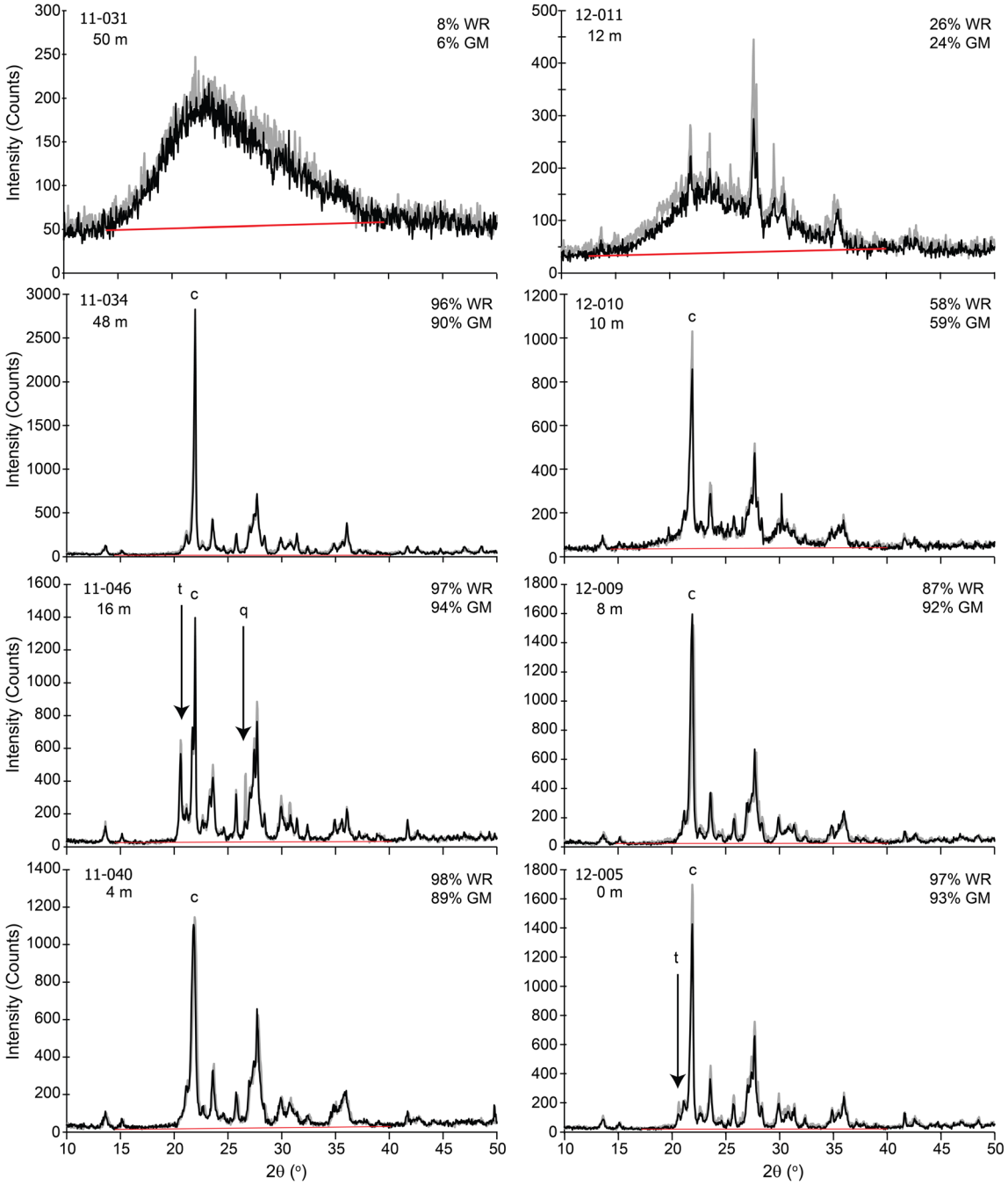

Fig. 3 X-ray diffraction patterns for selected whole rock (*grey*) and groundmass (*black*). Samples from BW section (11-prefix; *left*), and MC section (12-prefix; *right*). Linear background position indicated by the *red line*. 100 % peak intensity positions for quartz, cristobalite and tridymite are shown where present in the samples

In contrast to the BW section, the transition from crystallised interior to the upper vitrophyre is gradational for the 'thin' Monument Canyon section. Whole rock and groundmass crystallinity of the vitrophyre at the top of the MC section is ~26 %, significantly higher than the BW section. However, the presence of spherulites in the upper vitrophyre indicates at least minor crystallisation may have already affected these measurements. From the top down in the MC section, an increase in groundmass crystallinity from 24 to 92 % occurs over the course of 4 m. This same transition occurred in less than 1 m in the BW section. Groundmass crystallinity remains high (>90 %) throughout the remainder of the MC section down to the base, where no vitrophyre is exposed, and the difference between whole rock and groundmass crystallinity lacks the consistency observed in the BW section. The MC section displays a significant variation in

groundmass texture within an individual sample, even at the microscopic level. The non-systematic differences between groundmass and bulk crystallinity are attributed to these textural variations. Despite this, the similarity between the groundmass and whole rock measurements reinforces the robustness of overall trends in crystallinity through the sections.

Architecture of groundmass mineralogy

In the BW section of the ignimbrite, the groundmass mineralogy changes in a systematic fashion while passing vertically through the ignimbrite sheet (Fig. 4). At the base of the ignimbrite is a glassy vitrophyre with microlites of mafic phases (Fe-Ti oxides and pyroxene), formed in response to rapid chilling of the hot pyroclasts against the ground (i.e. the inferred fastest cooling rate). Directly above the basal vitrophyre, the groundmass mineralogy is dominated by crystallisation of a silica phase (predominantly cristobalite), Ca-rich feldspar and Na-K-rich feldspar (e.g. Rowe et al. 2012). Silica polymorphs are of particular interest because the appearance of different phases from the same initial material reflects variability in the time-temperature paths at different locations in the deposit. Cristobalite persists as the only groundmass silica phase until above 4 m height from base after which tridymite is also present. Between heights of 8–36 m tridymite is present as a second major silica phase with proportions ranging from 5 to 35 % of the total silica phase componentry. Quartz appears sporadically in the groundmass based on XRD scans; however, it is only found in the interior and just below the tridymite+cristobalite zone (Fig. 4). The lowermost occurrence of quartz is at a height of 4 m within the cristobalite zone where it comprises ~24 % of the total silica componentry, significantly higher than quartz proportions observed higher in the section. Within the tridymite zone, quartz proportions fluctuate from 2 to 7 %. The variation in silica phases is not symmetrical through the deposit with the cristobalite-only top portion significantly thicker compared to at the base. Additionally, tridymite proportions are non-symmetrical, with the highest proportions from 16 to 20 m section height (~35–29 %, respectively). The MC section has a distinctive pattern of silica phases compared to the BW section. The lowermost sample of the deposit is dominated by cristobalite and tridymite silica phases up to a height in the section of 4 m, at which point the remainder of the deposit only contains cristobalite (barring the uppermost vitrophyre). No quartz is evident in the MC section.

Groundmass textures

Although there is little systematic variation in crystallinity through the pervasively crystallised segment of the BW section, a textural evolution is apparent. Samples from near the top and base of the BW section of the ignimbrite contain in general much smaller crystal sizes and exhibit 'felty' textures,

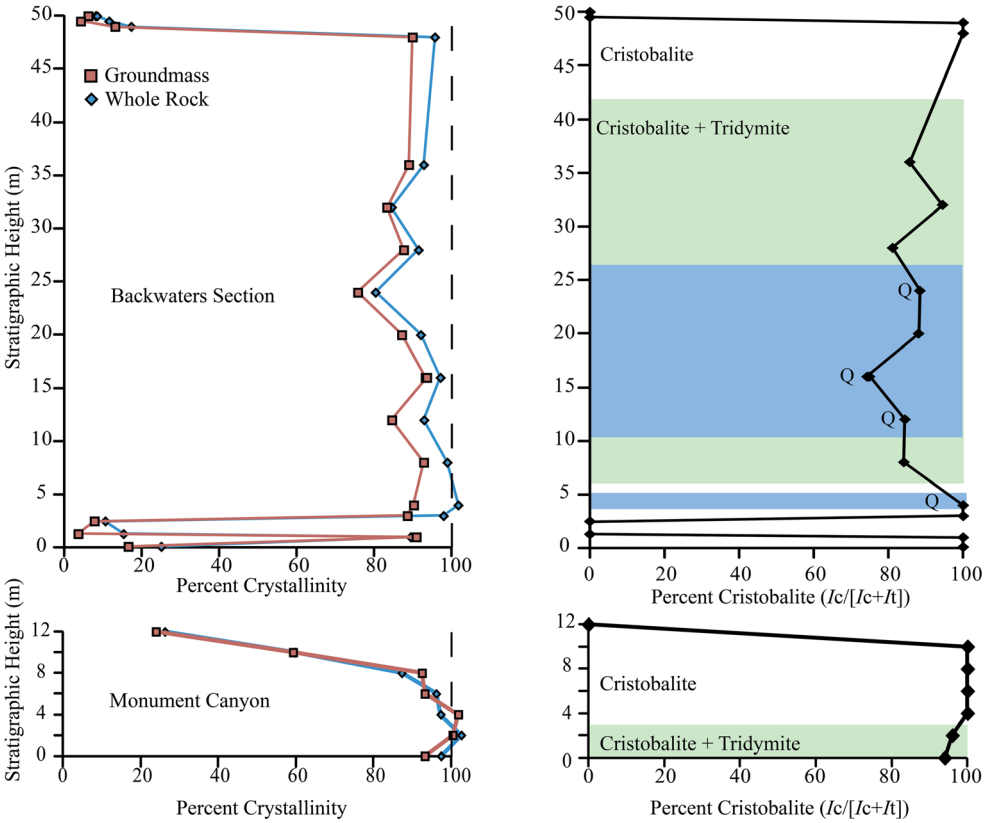

Fig. 4 X-ray diffraction **a** crystallinity results and **b** cristobalite proportion of the silica polymorphs as a function of stratigraphic height in the BW and MC sections. Appearance and abundance of quartz is sporadic, and excepting a lower quartz-rich zone, relatively minor, so proportions are calculated only from the intensity (counts) of X-rays associated with cristobalite ((*Ic* at 36.05 2*θ*)/0.13) and tridymite (*It* at 20.6 2θ) (e.g. 100 % means entirely cristobalite). The cristobalite> tridymite zone is indicated in *green* while the quartz-bearing zones are indicated in *blue* (with quartz-bearing samples indicated by 'Q')

similar to those identified by Rowe et al. (2012). Notably, there is no evidence for crystallisation overprinting textures inherited from glass (e.g. perlitic cracks) indicating direct crystallisation from a liquid on the surface rather than crystallisation following solidification to a glass. While samples near the top and bottom of the section have a matrix of fine, randomly oriented microlites, on passing towards the centre of the ignimbrite, groundmass textures become more mature, defined by a coarsening of grains (>50 μm, Fig. 5). Grain shape also changes with distance towards the centre. Near the upper and lower margins of the ignimbrite, no obvious grain morphologies are evident in the groundmass, except prismatic plagioclase of <10 μm size. Towards the interior, feldspar microlites become evident, in some cases retaining their near-euhedral morphology. With grain coarsening, in the middle of the ignimbrite, feldspar morphology is eliminated and large laths (up to 100 μm length) of a silica phase dominate, commonly found in a radiating geometry around a fine-grained silica–feldspar core. The space between the laths is filled by a matrix of feldspar of variable composition, with Na, Ca-rich feldspar (plagioclase) dominant near the centres of the radial features as well as in the cores of individual feldspar crystals. Crystal rims and distal areas are commonly dominated by K-rich feldspar (Fig. 5).

Geochemistry

Whole rock compositions

Bulk compositions are rhyolitic, ranging between 73.4 and 75.8 wt.% SiO_2 (recalculated anhydrous) identical to previous analyses of the Grey's Landing ignimbrite (e.g. Bonnichsen et al. 2008). XRF results (Fig. 6) indicate that, like most ignimbrites in the CSRP, the Grey's Landing is broadly compositionally homogeneous, both in vertical and lateral senses (Ellis et al. 2013). The glassy and microcrystalline samples

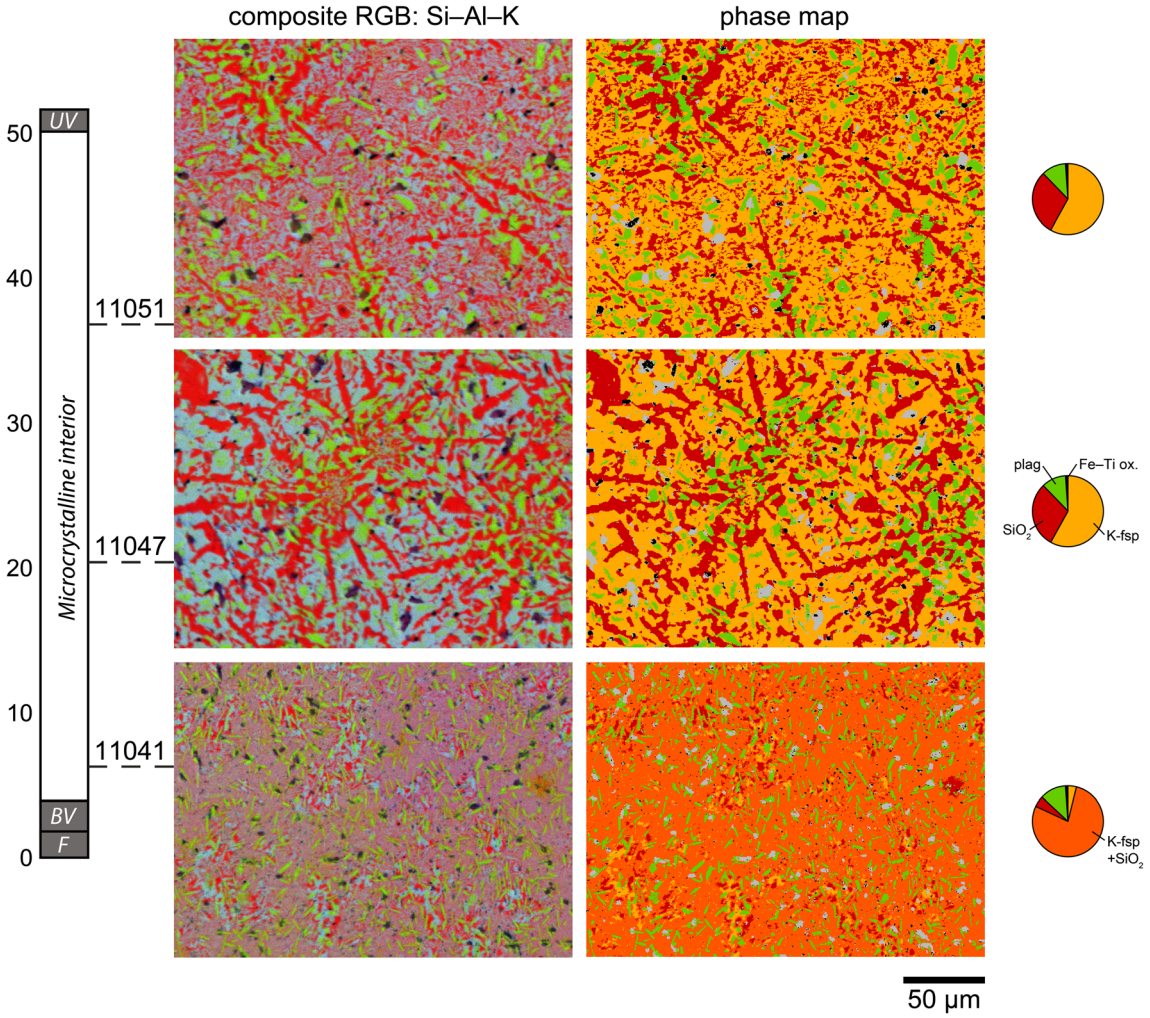

Fig. 5 Groundmass textures of three microcrystalline samples from the BW section, visualised by a combination of three intensity maps for Si (*red*), Al (*green*) and K (*blue*) as well as groundmass phase maps following classification with the iSpectra toolbox (Liebske 2015). All maps have the same scale. Pie charts illustrate the phase proportions calculated from respective phase maps with omission of unassigned pixels representing sample surface imperfections (shown in *grey* on phase maps)

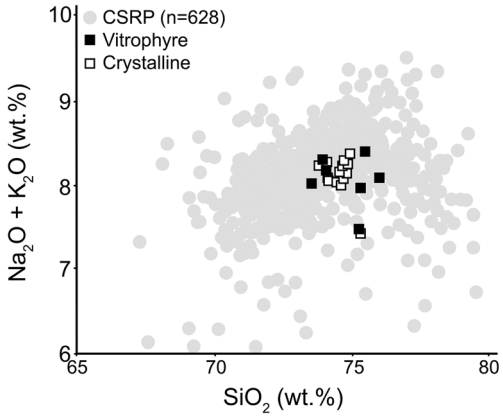

Fig. 6 Bulk rock compositions of Grey's Landing ignimbrite and ash (recalculated anhydrous) illustrating it is a typical CSRP rhyolite, with data from Bonnichsen et al. (2008)

vary in terms of their original totals with the microcrystalline samples having higher original totals (average 98.1, n=18) compared to the glassy samples (average 96.4 %, n=6). The other variations are seen in the alkali ratios which are affected by hydration of the glass, leading to lower Na/K ratios in the glassy samples. The limited compositional variability suggests that the processes which occur during crystallisation do not involve large-scale migrations of chemical constituents, in agreement with earlier studies (e.g. Bonnichsen et al. 2008; Rowe et al. 2012; Fig. 6).

Trace elements in glass

Rhyolitic glass from dense basal and upper vitrophyres of the Grey's Landing ignimbrite is identical in trace elemental composition. This homogeneity in trace elements indicates little compositional zonation within the magma prior to eruption (Ellis et al. 2013) and supports the use of trace elemental compositions in glasses as a correlation tool for Snake River Plain tephras (Perkins and Nash 2002). Rare earth element (REE) patterns within the Grey's Landing glasses show a characteristic negative Eu anomaly, and trace element abundances (Sr 45–87 ppm; Ba 1050–1230 ppm) are comparable with other SRP rhyolites (Ellis et al. 2013). Li contents within the glasses are also identical with the base containing 21–26 ppm and the top 17–26 ppm.

Trace elements in plagioclase

Plagioclase from vitrophyres at the top and bottom of the unit and from a number of locations within the crystallised interior were analysed, and as with trace elemental compositions in glasses, the abundances of almost all trace elements within plagioclase remain consistent in all samples throughout the BW section. The important exception to this lies with lithium. In plagioclase from the vitrophyres and the glassy fallout, Li contents range between 2 and 10 ppm (average=5, n=262). By contrast, within the crystallised interior of the ignimbrite, the plagioclase has much higher Li contents reaching 68 ppm (average=33, n=773), nearly an order of magnitude increase on that within the glassy samples (Figs. 7 and 8).

As shown in Fig. 7, the variability observed in Li in plagioclase between grains from microcrystalline and glassy samples is not mirrored in other trace elements such as Sr or Rb. The variability in Li within a sample cannot be ascribed to the analysis of another phase (i.e. inclusions) during the LA-ICPMS because the variation in Li shows no correlation with any other trace element and the integrations from the raw counts per second data provide stable homogeneous signals.

When individual plagioclase grains are investigated in more detail, the distribution of Li becomes increasingly complex (Fig. 9). Plagioclase from the glassy samples both at the base and the top of Grey's Landing exhibit significantly more homogeneous distributions of Li than those from the microcrystalline interior of the ignimbrite. An interesting feature of the data presented in Fig. 9 is the plagioclase grains from the

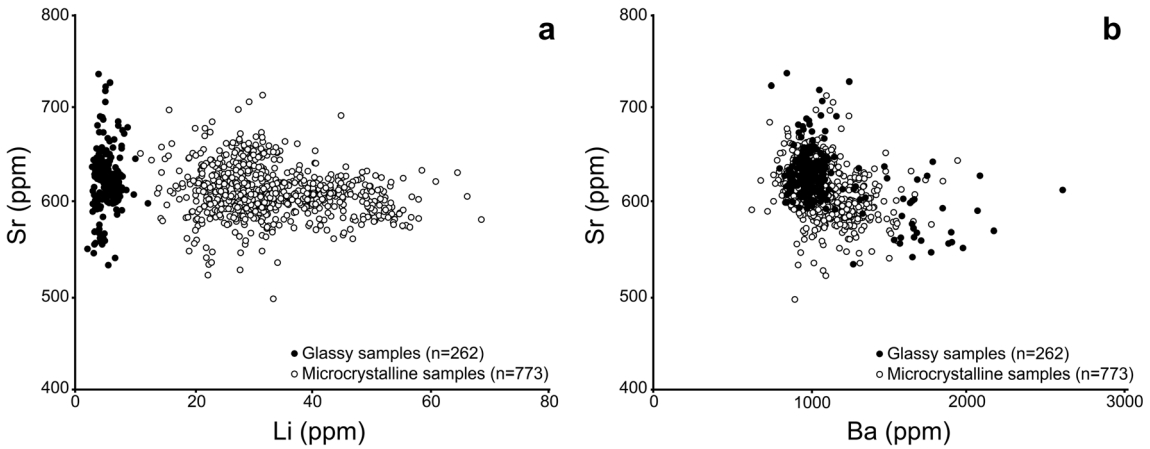

Fig. 7 Trace elemental compositions of Grey's Landing plagioclase phenocrysts distinguished by host lithology. **a** Glassy and microcrystalline samples overlap in terms of Sr contents but differ markedly in Li. **b** The two populations completely overlap in all other trace elements measured with Sr vs. Ba shown here

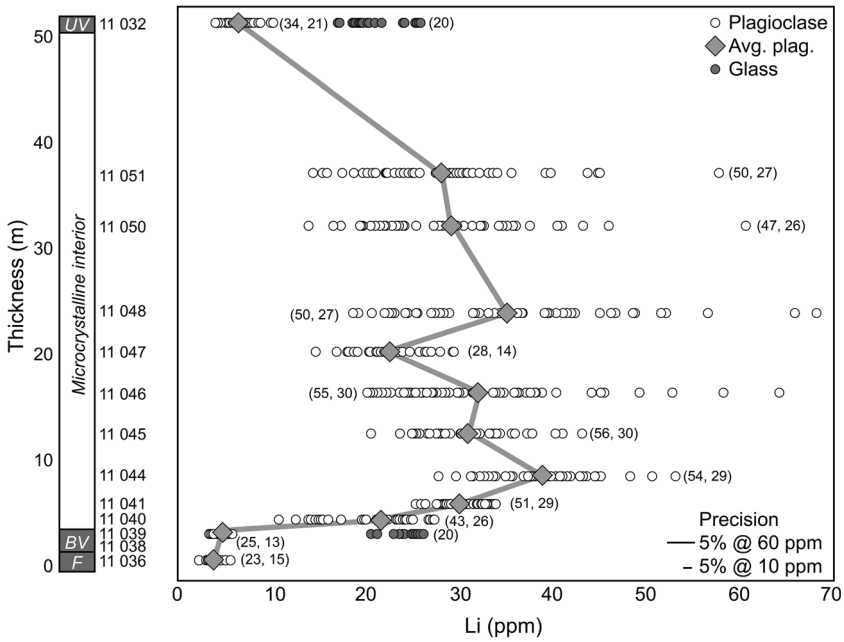

Fig. 8 Stratigraphic variation in Li content in plagioclase phenocrysts from the BW section of the Grey's Landing ignimbrite. Li contents from the glasses at the base and top of the ignimbrite are also shown to illustrate the lack of compositional zonation of 'initial Li contents' in the deposit. *Numbers* in parentheses represent the number of analyses from that sample and the number of grains analysed. *Thick grey line* represents the average of the data for each sample

microcrystalline interior show a relative depletion of Li (albeit still always higher than in the vitrophyre plagioclase) in the rims of the grains relative to the cores.

Numerical models

To constrain the cooling history of the Grey's Landing ignimbrite, we carried out numerical simulations with a range of starting conditions for various thicknesses of deposits (50, 12 and 3 m). Within these models, we assume that emplacement occurs both instantaneously and at an initial temperature (T_0), an assumption justified by the relatively short timescales of emplacement, inferred as a few days (Wilson 2008) to even tens of minutes (Lavallée et al. 2015), compared to the characteristic time scale of cooling (order of years). Among other variable parameters, those explicitly tested within these models include the initial temperature from which cooling starts, the density of nucleation sites and the growth rates of crystals.

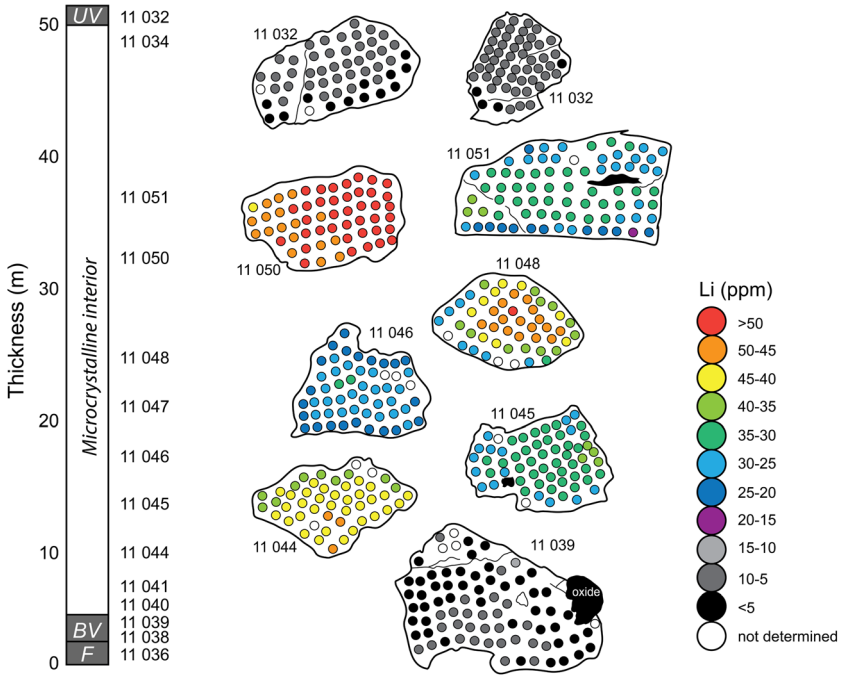

Fig. 9 Stratigraphic section of Grey's Landing ignimbrite showing grains studied in detail for the distribution of Li. As illustrated in Fig. 7, plagioclase from the interior of the ignimbrite always contains more Li than plagioclase from the vitrophyres

Temperatures used for models span a few hundred degrees including those similar to magmatic temperatures inferred via geothermometry (Andrews et al. 2008) and encompass potentially higher initial temperatures resulting from shear heating during syn-depositional rheomorphism (Cordonnier et al. 2012; Robert et al. 2013) and lower temperatures reflecting possible cooling of the pyroclasts during transport. The nucleation density (N_0) of the groundmass has been estimated from final crystal density observations (5×10^{13} m^{-3}), but a range (10^{11} to 10^{14} m^{-3}) has been tested to consider the variability observed along the profile as well as uncertainty linked to inhomogeneity of samples. Observations indicate higher crystal density for areas crystallised at high cooling rate (i.e. high undercooling conditions) while crystals grown under low cooling rate exhibit lower crystal density (i.e. low undercooling conditions). Crystal growth rates in rhyolites remain poorly constrained (Swanson 1977, Zhang 2013 and references therein). As is clear from above, the dominant minerals in the groundmass of the Grey's Landing ignimbrite are silica phases and potassic feldspar with subsidiary plagioclase. Given the large uncertainties on quartz and sanidine growth rates for magmatic conditions, and the lack of data for surficial conditions, we use the crystal growth rates estimated by Castro et al. (2008) from water diffusional profiles next to spherulites which range from 5×10^{-10} up to 5×10^{-9} m s^{-1}. The spherulites in their study were dominated by plagioclase rather than quartz and potassic feldspar, but these values best reflect the conditions of interest. Crystal growth rate has been historically constrained by three major models. The isothermal linear growth model of Keith and Padden (1963) assumes a constant growth rate and neglects crystal size or variations of the melt chemical composition. The size and temperature dependent growth model of Castro et al. (2008) remains empirical and must be extrapolated for large crystal size; hence, a slower crystallisation rate may be expected. Finally, the diffusion controlled model of Watkins et al. (2009) inspired by Gránásy theory (Gránásy et al. 2005) remains the most physically correct existing model but is not self-limiting and by considering an infinite medium around the crystal, it may overestimate crystal growth at large crystal fractions. For this work, we tested a crystal size/temperature controlled growth models as described by Castro et al. (2008). A 1D finite difference cooling model with crystal growth, as described in Supplemental Material, is used to estimate crystal fraction, temperature and cooling rate of the different profiles investigated. Earlier simulations (Manley and Andrews 2004; Andrews 2006) did not account for crystallisation, groundmass mineralogy and latent heat production.

Given that the Grey's Landing ignimbrite is well-exposed, we can use field observations as constraints on our numerical simulations. For any simulation to be accepted, it must match the following observations; (1) where the ignimbrite is thick (i.e. ~50 m), the thickness of the lower and upper vitrophyres are required to be respectively in the range 1.5–2 and 3–5 m. When the ignimbrite is 12 m thick, the thickness of the lower and upper vitrophyres is required to be respectively in the range 1–2 and 2–3 m. Where the ignimbrite is thin (i.e. ~3 m thick as it is near Highway 93; Fig. 1), the entire ignimbrite should be glassy (e.g. Andrews et al. 2008; Andrews and Branney 2011).

Overall, simulations display a strong contribution of latent heat during crystallisation process; the thinner the deposit, the more cooling affects the whole profile before latent heat reheats the ignimbrite. Latent heat only affects profiles where temperature is maintained long enough for crystals to grow; for a cooling rate greater than $10^{-4.5}$ K s^{-1}, rhyolite cools too fast to allow crystals to grow, suggesting a cooling rate between the $10^{-2.8}$ K s^{-1} derived from experimental work (Lavallée et al. 2015) and the $10^{-4.5}$ K s^{-1} derived from our models for the Snake River Plain vitrophyres.

The best fit of simulations (all simulations are provided in Supplemental Material S2) came from an initial emplacement temperature of T_0=900 °C and a crystal growth rate of a quarter of the model of Castro et al. (2008) and is able to reproduce the field observations in both BW and MC sections. In this model, the cooling rates for the upper and basal vitrophyres range between $10^{-2.8}$ and $10^{-4.5}$ K s^{-1} and are approximately 10^{-6} K s^{-1} for the crystalline lithology. As a comparison, Gottsmann and Dingwell (2001) used differential scanning calorimetry to quantify the cooling rate of rhyolitic glass from Rocche Rosse flow of Lipari, with modelled cooling rates in the range of $10^{-2.4}$ to $10^{-3.3}$ K s^{-1}. While the Rocche Rosse lava was emplaced at a somewhat lower temperature than the Grey's Landing ignimbrite, the cooling rates inferred in that study closely match the cooling rates returned via our numerical models when set for similar conditions and are concordant with the cooling rates of the glassy portions of the Grey's Landing.

Discussion

Cooling and crystallisation of rhyolite at the surface

The variability in thickness of the Grey's Landing ignimbrite and the pristine condition of the deposits allow the post-depositional processes to be investigated. The first-order differences in cooling rates are illustrated in the glassy or crystalline nature of the lithology, but microscopic textures (e.g. Fig. 5) illustrate the more subtle effects of variations in cooling rates.

Conditions for rheomorphism

Rheomorphism occurs when a pyroclastic deposit agglutinates together during or immediately after deposition and

undergoes ductile deformation in some combination of non-coaxial shear strain in discrete shear zones and distributed coaxial shear strain during lateral spreading. When rheomorphism occurs has been a matter of debate with some favouring it being entirely post-depositional (Wolff and Wright 1981); during emplacement of an already thick 'plug' of ignimbrite (e.g. Schmincke and Swanson 1967; Chapin and Lowell 1979); while others have suggested it begins syn-depositionally during progressive aggradation of ignimbrite (e.g. Branney and Kokelaar 1992; Kobberger and Schmincke 1999; Andrews and Branney 2011). For rheomorphism to occur, the tuff must be capable of ductile flow at appropriate strain rates and timescales. The window for rheomorphism is therefore constrained by (1) passing through either the glass transition temperature (in the case of rapidly cooled samples which end up as glass, Stevenson et al. 2001; Giordano et al. 2005) or a crystallinity threshold (most commonly taken as ~40–45 % crystallinity; Bagdassarov et al. 1994; Stevenson et al. 1996), both of which represent an increase in effective viscosity of several orders of magnitude, and (2) the continued availability of gravitational disequilibrium to induce and sustain lateral flow.

Our numerical results, in good agreement with the experimental results of Lavallée et al. (2015), indicate that the glassy upper and basal margins of the Grey's Landing ignimbrite pass through the glass transition temperature and thus out of the 'rheomorphism window' rapidly. These simulations (Fig. 10) indicate that the interior of the deposit may remain at high temperatures when the outer portions have chilled to a glass (e.g. Romine et al. 2012). Considering location MC in Fig. 10 at time of 0.5×10^8 s (slightly less than 2 years), it is clear that both the upper and lower vitrophyres are solid glasses with temperatures of less than 500 °C (and in the case of the upper vitrophyre, significantly less than this) while the interior of the ignimbrite remains hot (>900 °C) with a crystal fraction of about 0.3–0.4. Thus, where the Grey's Landing ignimbrite ponded in the Rogerson Graben, location BW, the interior of the deposit remained capable of rheomorphism long after the upper, lower, and lateral margins were solid. Where the other end member is considered, at location H (Fig. 10), the whole deposit is cooler than 600 °C after 0.5×10^6 s (approximately 1 week).

These numerical models support the intuitive conclusion that the end of the rheomorphism window is diachronous both laterally through a deposit sheet and vertically in a single location. This is supported by field evidence for rheomorphic flow of the Grey's Landing ignimbrite at several locations. At Salmon Falls dam ('S', Fig. 1), the competent upper vitrophyre brecciated during post-depositional folding of the adjacent incompetent ignimbrite core (now microcrystalline; Andrews and Branney 2011). Near the Highway 93 and Monument Canyon localities, the competent upper vitrophyre is extended along brittle listric normal faults that root into the underlying microcrystalline core, providing evidence of shear-thinning of the deposit as insulated, hot material in the core was able to flow laterally (Andrews 2006). Where the Grey's Landing ignimbrite is ponded, its upper surface is remarkably planar and close to horizontal. In contrast, where it is thin and mantles the underlying paleoslopes, the upper surface of the ignimbrite contains relief caused by rheomorphic folding. This is interpreted as a manifestation of the thickness-controlled diachroneity discussed here, and indeed, the transition from topographic-mantling to topographic-filling behaviour corresponds fairly well to the 8-m isopach (Andrews 2006). Rheomorphism in the core of the ponded Grey's Landing ignimbrite was likely arrested by the deposit attaining gravitational equilibrium through post-depositional rheomorphic flow. Conversely, rheomorphism in thin marginal locations was arrested by quenching of vitrophyres and crystallisation of the thin ignimbrite cores in the margins before gravitational equilibrium was achieved.

Li in the post-depositional realm

The behaviour of Li in silicic magmatic systems at high temperature remains poorly known. The classic early studies of trace element partitioning typically could not measure Li in mineral phases (e.g. Mahood and Hildreth 1983; Nash and Crecraft 1985), and more recent studies typically used less evolved compositions and much higher temperatures than those of rhyolite emplacement (e.g. with lowest temperatures of 1153 °C; Bindeman et al. 1998). Furthermore, there remains disagreement about the extent to which the anorthite content of the plagioclase plays a role in terms of partitioning with some authors suggesting the effect is negligible (Bindeman et al. 1998) and others suggesting it is important (Coogan 2011). A large variability in Li contents in plagioclase (and resultantly large variations in K_D values for Li) has long been observed (Smith and Brown 1988). The rapid diffusion of Li has been utilised by a number of studies to capture near and syn-eruptive processes occurring on shorter timescales than most geochemical tracers record (Berlo et al. 2004; Kent et al. 2007; Charlier et al. 2012). For these reasons, we do not claim that the Li contents of the glass represent the pre-eruptive magmatic liquid as Li may have degassed during the explosive eruption; rather, we consider the glassy portions of the Grey's Landing deposit to represent the conditions immediately at emplacement of the deposit. The distribution of Li in the glassy portions of the Grey's Landing ignimbrite is simple with both glass and plagioclase homogeneous in Li and containing an average of 23 and 5 ppm, respectively. By contrast, the Li contents of plagioclase from the interior of the ignimbrite show significantly more variability, suggesting that they record a more complicated suite of processes.

Studies of hundreds of bulk rocks analyses from CSRP rhyolites reveal no systematic differences between the bulk

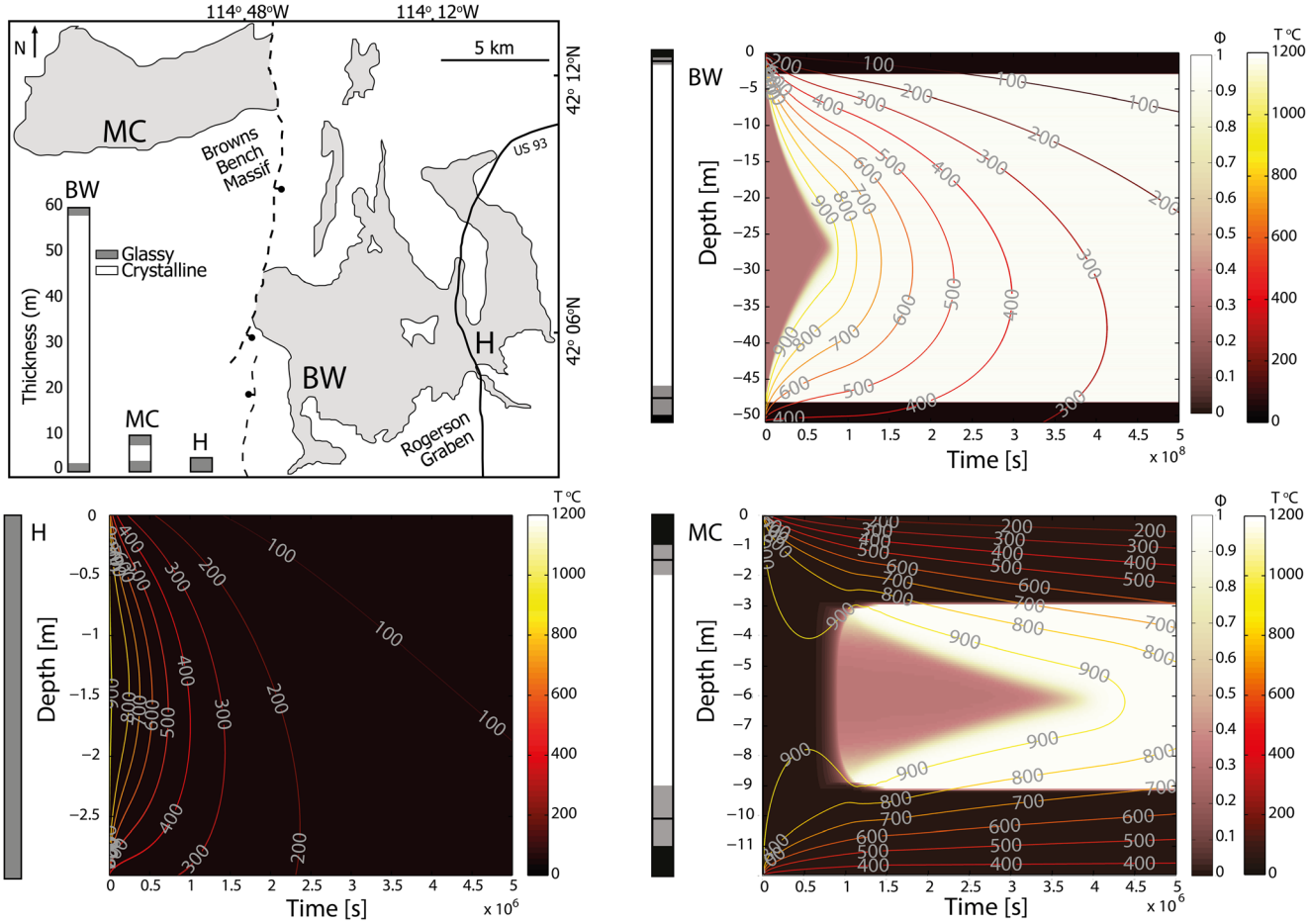

Fig. 10 Diagram illustrating the ability of our crystallisation model to replicate field observations from three locations with different thicknesses of Grey's Landing. *Black* indicates amorphous material, and *white* indicates fully crystalline material while temperature contours illustrate the temperature of the relative positions in the ignimbrite as a function of time. Note that the time axis for location BW is two orders of magnitude longer than that shown for H and MC. On panels termed Geol, the *black* reflects glassy material, the *grey* is potential uncertainty on field observations and white reflects fully crystalline

compositions of microcrystalline and glassy samples of the same unit (Bonnichsen et al. 2008; Ellis et al. 2013; data above). Thus, we can confidently state that groundmass crystallisation does not cause large scale migration of major elements. Maintenance of a high-silica rhyolitic composition during crystallisation (as in the glass) requires that the main phases crystallising must be sanidine, quartz (or a polymorph) and plagioclase. By making simple mass balance models (e.g. Fig. 11) using typical CSRP mineral compositions, we can estimate the relative proportions of phases that crystallise. We note here that the composition of phases in the microcrystalline portion of Grey's Landing may be slightly different to those taken as typical CSRP compositions, but such variability would not be expected to make large changes in the results. As illustrated in Fig. 11, the relatively high K_2O content of Grey's Landing glasses (>5 wt.%) requires abundant K-feldspar crystallisation, with the best matches to real compositions coming with 50–60 % groundmass K-feldspar. Phase proportions derived from maps presented in Fig. 5 agree with this

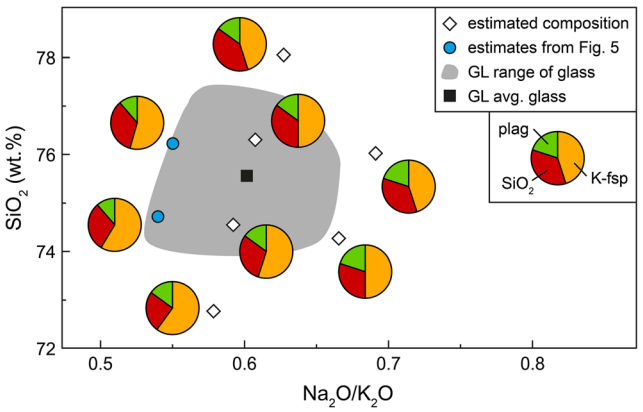

Fig. 11 Diagram reconstructing the composition of Grey's Landing glass from various proportions of the phases produced during groundmass crystallisation, as illustrated by pie charts. Composition of plagioclase and sanidine used are typical of SRP feldspars (e.g. Ellis et al. 2013), and we note that slight differences do not significantly change the mineral proportions required. Compositions generated from phase proportions do not include the influence of small proportions of Fe-Ti oxides

conclusion; using the same typical compositions of each phase (Fig. 11).

The high proportion of sanidine crystallised in the groundmass may provide an explanation for the elevated Li in plagioclase phenocrysts from the microcrystalline samples. Where we have measured Li contents in plagioclase and sanidine phenocrysts, and co-existing glass from other Snake River Plain rhyolites (Szymanowski 2014), Li has a significantly higher affinity for plagioclase than for sanidine. Li contents of sanidine are typically low (2–4 ppm) with plagioclase values approximately three times greater and glass nearly an order of magnitude larger. The low affinity of Li for sanidine may explain why as the rhyolitic melt begins to crystallise the (now excess) Li diffuses into the plagioclase phenocrysts. The role of the silica-rich phase (be it quartz, tridymite or cristobalite) remains poorly known, but the behaviour of sanidine allows a qualitative model to be suggested for the newly reported behaviour of Li in plagioclase.

A synoptic view of post-eruptive crystallisation

By comparing the data from the multiple techniques together, we can infer what the different data sets are revealing. In terms of crystallinity, aside from one sample at the MC location, the results are bimodal with samples either highly crystalline (bulk >85 % crystalline) or glassy. This suggests that once crystallisation of the groundmass starts, it typically proceeds to completion. Such a step function in crystallisation is predicted by our numerical models where the boundary between ~30 % crystalline (pink in Fig. 10) and fully crystalline (white in Fig. 10) is typically sharp. By contrast, the groundmass texture and mineralogy of the ignimbrite do appear to change in concert with the amount of time spent at high temperature. Near the base of the crystalline portion of BW section, the texture is fine-grained and felty, dominated by quartz and cristobalite with plagioclase microlites. In the centre of the ignimbrite (Fig. 5), the textures are notably different with coarser-grained silica phases and plagioclase found in distinct clusters.

The behaviour of Li in the deposit does not appear to show a perfect relationship with cooling rate (Fig. 8). When considering just the microcrystalline interior of the deposit, the samples from closest to the vitrophyre show smaller ranges of Li than those from the core of the BW section. This, along with the relatively Li-depleted rims of plagioclase (Fig. 9), suggests complex behaviour of Li following deposition. While our dataset of >1000 analyses of Li in plagioclase (see sup. materials) illustrates for the first time the variability existing through a single ignimbrite, it merely scratches the surface in terms of understanding the processes ongoing during crystallisation on the surface. We suggest understanding the behaviour of Li in slowly cooled volcanic deposits would be a fruitful avenue for further investigations.

Conclusions

The well-preserved Grey's Landing ignimbrite provides an opportunity to study in detail the emplacement and post-emplacement processes associated with voluminous, high-grade ignimbrite eruptions. Our study leads us to conclude the following:

1) Overall, the Grey's Landing ignimbrite is a compositionally homogeneous deposit, both vertically and laterally. The notable exception to this homogeneity is observed in plagioclase crystals where Li, and only Li, shows significant variability on the order of magnitude scale. This stark variability correlates with the groundmass texture with plagioclase from rapidly cooled, glassy groundmass samples having low Li abundances (average 5 ppm, n= 262) whereas those from the more slowly cooled interior of the ignimbrite have higher Li abundances (average 33 ppm, n=776). Glass and whole rock compositions from the base and top of the unit indicate that such variability in Li is not magmatic and must represent a post-emplacement process. These results require that any studies of the behaviour of Li in volcanic rocks must be accompanied by consideration of the cooling history of the deposit.
2) Associated with the variability in Li abundances in plagioclase, the Grey's Landing ignimbrite exhibits variability in both texture and mineralogy of the groundmass. On passing from the margins to the centre of the ignimbrite, the crystals become larger and tridymite and quartz join cristobalite as the SiO_2 phase in the groundmass.
3) Numerical models of cooling and crystallisation, in good agreement with previous models based on differential scanning calorimetry, suggest that rheomorphism must be a rapid process in the vitrophyres. In the slowly cooled interior, it can persist for a few years at which point high degrees of crystallinity limit the ability to flow, even if gravitational disequilibrium is maintained. Our work provides further support for recent studies that conclude rheomorphism is syn-depositional. Furthermore, we show that the rheomorphism window is diachronous across a single ignimbrite sheet and dependent on the time-temperature path of the deposit at that location.

Acknowledgments We would like to thank the GeoAnalytical Laboratory at Washington State University for providing first class geochemical data as ever. LA-ICPMS analyses were facilitated by the excellence of Marcel Guillong, and XRD data were collected with the help of Abbie Lindeberg. We appreciate the constructive reviews of Christoph Breitkreutz and an anonymous reviewer as well as the editorial effort from Steve Self. Partial financial support for this project from NSF (USA) EAR-0911457 and HRD-1137774, and SNSF – 200021_155923 (Switzerland) is gratefully acknowledged.

References

Andrews GDM (2006) The emplacement and deformation of high-temperature tuffs: a structural analysis of the Grey's Landing ignimbrite, Snake River Plain, Idaho. Unpub PhD thesis, Univ Leicester, 337 pages

Andrews GDM, Branney MJ (2011) Emplacement and rheomorphic deformation of a large, lava-like rhyolitic ignimbrite: Grey's Landing, southern Idaho. Geol Soc Am Bull 123:725–743. doi:10.1130/B30167.1

Andrews GDM, Branney MJ, Bonnichsen B, McCurry M (2008) Rhyolitic ignimbrites in the Rogerson Graben, southern Snake River Plain volcanic province: volcanic stratigraphy, eruption history and basin evolution. Bull Volcanol 70:269–291. doi:10.1007/s00445-007-0139-0

Bagdassarov ND, Dingwell DB, Webb SL (1994) Viscoelasticity of crystal- and bubble-bearing rhyolite melts. Phys Ear Plan Inter 83: 83–99

Baxter PJ, Bonadonna C, Dupree R, Hards VL, Kohn SC, Murphy MD, Nichols A, Nicholson RA, Norton G, Seal A, Sparks RSJ, Vickers BP (1999) Cristobalite in volcanic Ash of the Soufriere Hills Volcano, Montserrat, British West Indies. Science 283:1142–1145

Berlo K, Blundy J, Turner S, Cashman K, Hawkesworth C, Black S (2004) Geochemical precursors to volcanic activity at Mount St. Helens, USA. Science 306(5699):1167–1169. doi:10.1126/science.1103869

Bindeman IN, Davis AT, Drake MJ (1998) Ion microprobe study of plagioclase-basalt partition experiments at natural concentration levels of trace elements. Geochem Cosmochem Acta 62(7):1175–1193

Bonnichsen B, Leeman WP, Honjo N, McIntosh WC, Godchaux MM (2008) Miocene silicic volcanism in southwestern Idaho: geochronology, geochemistry, and evolution of the central Snake River Plain. Bull Volcanol 70:315–342. doi:10.1007/s00445-007-0141-6

Boroughs S, Wolff JA, Ellis BS, Bonnichsen B, Larson PB (2012) Evaluation of models for the origin of Miocene low-$\delta^{18}O$ rhyolites of the Yellowstone/Columbia River Large Igneous Province. Earth Planet Sci Lett 313–314:45–55

Branney MJ, Kokelaar P (1992) A reappraisal of ignimbrite emplacement: progressive aggradation and changes from particulate to non-particulate flow during emplacement of high-grade ignimbrite. Bull Volcanol 54:504–520

Branney MJ, Bonnichsen B, Andrews GDM, Ellis B, Barry TL, McCurry M (2008) 'Snake River (SR) -type' volcanism at the yellowstone hotspot track: distinctive products from unusual, high-temperature silicic super-eruptions. Bull Volcanol 70:293–314. doi:10.1007/s00445-007-0140-7

Brueseke ME, Hart WK, Heizler MT (2008) Diverse mid-Miocene silicic volcanism associated with the Yellowstone–Newberry thermal anomaly. Bull Volcanol 70:343–360

Cashman KV, Thornber CR, Pallister JS (2008) From dome to dust: shallow crystallisation and fragmentation of conduit magma during the 2004–2006 dome extrusion of Mt. St. Helens, Washington. US Geol Surv Prof Paper 1750:387–413

Castro JM, Beck P, Tuffen H, Alexander RL, Dingwell DB, Martin C (2008) Timescales of spherulite crystallization in obsidian inferred from water concentration profiles. Am Mineral 93:1816–1822

Castro JM, Cottrell E, Tuffen H, Logan AV, Kelly KA (2009) Spherulite crystallization induces Fe-redox redistribution in silicic melt. Chem Geol 268:272–280

Chapin CE, Lowell GR (1979) Primary and secondary flow structures in ash-flow tuffs of the Gribbles Run paleovalley, central Colorado. In Chapin CE, Elston WE (eds) Ash-flow tuffs. Geol Soc Am Spec Pap 180:137–154

Charlier BLA, Morgan DJ, Wilson CJN, Wooden JL, Allan ASR, Baker JA (2012) Lithium concentration gradients in feldspar and quartz record the final minutes of magma ascent in an explosive supereruption. Earth Plan Sci Lett 319–320:218–227. doi:10.1016/j.epsl.2011.12.016

Coogan LA (2011) Preliminary experimental determination of the partitioning of lithium between plagioclase crystals of different anorthite contents. Lithos 125(1–2):711–715. doi:10.1016/j.lithos.2011.03.016

Cordonnier B, Schmalholz SM, Hess K-U, Dingwell DB (2012) Viscous heating in silicate melts: an experimental and numerical comparison. J Geophys Res 117, B02203. doi:10.1029/2010JB007982

Ellis BS, Barry TL, Branney MJ, Wolff JA, Bindeman I, Wilson R, Bonnichsen B (2010) Petrologic constraints on the development of a large-volume, high temperature, silicic magma system: the Twin Falls eruptive centre, central Snake River Plain. Lithos 120:475–489. doi:10.1016/j.lithos.2010.09.008

Ellis BS, Wolff JA, Boroughs S, Mark DF, Bonnichsen B, Starkel WA (2013) Rhyolitic Volcanism of the central Snake River Plain: a review. Bull Volcanol 75:745. doi:10.1007/s00445-013-0745-y

Gardner JE, Befus KS, Watkins J, Hesse M, Miller N (2012) Compositional gradients surrounding spherulites in obsidian and their relationship to spherulite growth and lava cooling. Bull Volcanol 74:1865–1879

Geist D, Richards MA (1993) Origin of the Columbia plateau and the Snake River Plain: deflection of the Yellowstone plume. Geology 21:789–792

Giordano D, Nichol ARL, Dingwell DB (2005) Glass transition temperatures of natural hydrous melts: a relationship with shear viscosity and implications for the welding process. J Volcanol Geotherm Res 142:105–118

Gottsmann J, Dingwell DB (2001) The cooling of frontal flow ramps: a calorimetric study on the Rocche Rosse rhyolite flow, Lipari, Aeolian Islands, Italy. Terra Nov. 13:157–164. doi:10.1046/j.13653121.2001.00332.x

Gránásy L, Pusztai T, Tegze G, Warren JA, Douglas JF (2005) Growth and form of spherulites. Phys Rev E 72:011605. doi:10.1103/PhysRevE.72.011605

Hildreth W, Wilson CJN (2007) Compositional zoning of the Bishop Tuff. J Petrol 48:951–999. doi:10.1093/petrology/egm007

Horwell CJ, Le Blond JS, Michnowicz SAK, Cressey G (2010) Cristobalite in a rhyolitic lava dome: evolution of ash hazard. Bull Volcanol 72:249–253

Husain T, Elsworth D, Voight B, Mattioli G, Jansma P (2014) Influence of extrusion rate and magma rheology on the growth of lava domes: insights from particle-dynamics modeling. J Volcanol Geotherm Res 285:100–117

Keith HD, Padden FJ (1963) A phenomenological theory of spherulitic crystallization. J App Phys 34:2409. doi:10.1063/1.1702757

Kent AJR, Blundy J, Cashman KV, Donnelly C, Pallister JS, Reagan M, Rowe MC, Thornber CR (2007) Vapor transfer prior to the October 2004 eruption of Mount St. Helens, Washington. Geology 35(3): 231–234. doi:10.1130/G22809A.1

Kobberger G, Schmincke HU (1999) Deposition of rheomorphic ignimbrite D (Mogan Formation) Gran Canaria, Canary Islands, Spain. Bull Volcanol 60:465–485

Lavallée Y, Wadsworth FB, Vasseur J, Russell JK, Andrews GDM, Hess K-U, von Aulock FW, Kendrick JE, Tuffen H, Biggin AJ, Dingwell DB (2015) Eruption and emplacement timescales of ignimbrite super-eruptions from thermo-kinetics of glass shards. Front Earth Sci 3:2. doi:10.3389/feart.2015.00002

Liebske C (2015) iSpectra: an open source toolbox for the analysis of spectral images recorded on SEM–EDS systems. Microsc Microanal 21:1006–1016

Mahood G, Hildreth WA (1983) Large partition coefficients for trace elements in high-silica rhyolites. Geochim Cosmochim Acta 47: 11–30

Manley CR, Andrews GDM (2004) A numerical modelling investigation of the duration of post-emplacement rheomorphism in a high-grade ignimbrite: Grey's Landing, Idaho. Geol Soc Am Abs w Prog 36(4): 12. doi:10.1371/journal.pone.0044205

Nash WP, Crecraft HR (1985) Partition coefficients for trace elements in silicic magmas. Geochim Cosmochim Acta 49:2309–2322

Perkins ME, Nash BP (2002) Explosive silicic volcanism of the Yellowstone hotspot: the ash fall tuff record. Geol Soc Am Bull 114:367–381

Pick T, Tauxe L (1993) Geomagnetic palaeointensities during the Cretaceous normal superchron measured using submarine basaltic glass. Nature 366:238–242

Robert G, Andrews GDM, Ye J, Whittington AG (2013) Rheological controls on the emplacement of extremely high-grade ignimbrites. Geology 41:1031–1034. doi:10.1130/G34519.1

Romine WL, Whittington AG, Nabelek PI, Hofmeister AM (2012) Thermal diffusivity of rhyolitic glasses and melts: effects of temperature, crystals and dissolved water. Bull Volcanol 74: 2273–2287

Ross CS, Smith RL (1955) Water and other volatiles in volcanic glasses. Am Mineral 40(11–2):1071–1089

Rowe MC, Ellis BS, Lindeberg A (2012) Quantifying crystallization and devitrification of rhyolites via X-ray diffraction and electron microprobe analysis. Am Mineral 97(10):1685–1699

Schmincke H-U, Swanson DA (1967) Laminar viscous flowage structures in ash-flow tuffs from Gran Canaria, Canary Islands. J Geol 75: 641–664

Smith JV, Brown WL (1988) Feldspar Minerals. Vol. 1, Springer-Verlag, 841 pp

Stevenson RJ, Dingwell DB, Webb SL, Sharp TG (1996) Viscosity of microlite-bearing rhyolitic obsidians: an experimental study. Bull Volcanol 58:298–309

Stevenson RJ, Dingwell DB, Bagdassarov NS, Manley CR (2001) Measurement and implication of "effective" viscosity for rhyolite flow emplacement. Bull Volcanol 63:227–237

Swanson SE (1977) Relation of nucleation and crystal-growth rate to the development of granitic textures. Am Mineral 62:966–978

Szymanowski D (2014) Mineral-scale evolution of voluminous rhyolites of the Heise volcanic field, eastern Snake River Plain, Idaho, USA. MSc thesis, ETH Zürich

Szymanowski D, Ellis BS, Bachmann O, Guillong M, Phillips WM (2015) Bridging basalts and rhyolites in the Yellowstone–Snake River Plain volcanic province: the elusive intermediate step. Earth Plan Sci Lett 415:80–89

Wall KT, Rowe MC, Ellis BS, Schmidt ME, Eccles JD (2014) Determining volcanic eruption styles on Earth and Mars from crystallinity measurements. Nat Comm 5:5090

Watkins J, Manga M, Huber C, Martin M (2009) Diffusion-controlled spherulite growth in obsidian inferred from H_2O concentration profiles. Contrib Mineral Petrol 157:163–172

Wilson CJN (2008) Supereruptions and supervolcanoes: processes and products. Elements 4:29–34

Wolff JA, Wright JV (1981) Rheomorphism of welded tuffs. J Volcanol Geotherm Res 10:13–34

Wolff JA, Ramos FC, Hart GL, Patterson JD, Brandon A (2008) Columbia River flood basalts from a centralized crustal magmatic system. Nat Geosci 1:177–180

Zhang Y (2013) Kinetics and dynamics of mass-transfer-controlled mineral and bubble dissolution or growth: a review. Eur J Mineral 25: 255–266. doi:10.1127/0935-1221/2013/0025-2292